

Acoustic phonons in graphene nanoribbons

Matthias Droth* and Guido Burkard*

Department of Physics, University of Konstanz, 78457 Konstanz, Germany

E-mail: matthias.droth@uni-konstanz.de; guido.burkard@uni-konstanz.de

Abstract

Phonons are responsible for limiting both the carrier mobility and the spin relaxation time. In view of a possible transistor function as well as spintronics applications in graphene nanoribbons, we present a theoretical study of acoustic phonons in these nanostructures. Using a two-dimensional continuum model which takes into account the monatomic thickness of graphene, we derive hermitian wave equations as well as phonon creation and annihilation operators, thus allowing for a quantum mechanical treatment of the system. Two types of boundary configurations, which we believe can be realized in experiment, are discussed: (i) fixed and (ii) free boundaries. The former leads to a gapped phonon dispersion relation while the latter exhibits an ungapped dispersion relation and a finite sound velocity of out-of-plane modes at the center of the Brillouin zone. In the limit of negligible boundary effects, bulk-like behaviour is restored.

Graphene is a monatomic layer of carbon atoms arranged in a honeycomb lattice with two atoms per unit cell. Its interesting electronic and mechanical properties have made it a promising candidate for a wide range of applications including ballistic transistors as well as spintronics and nanoelectromechanical devices.^{1–5} There are, however, two drawbacks: (i) for epitaxial graphene,

*To whom correspondence should be addressed

which is desirable for a controlled, large scale production, the strong coupling to a substrate compromises these properties and (ii) graphene has no bandgap, a handicap for typical semiconductor applications.

The first challenge can be overcome by removing substrate material from underneath the carbon layer such that a trench is formed and the electronic properties of free-standing graphene are restored.^{6–10} The second challenge is met by graphene nanoribbons (GNRs), graphene strips with a width at the nanometer scale (e.g., $L \sim 1 \mu\text{m}$, $W \sim 30 \text{ nm}$) which can exhibit a bandgap.¹¹ Combining all these advantages, the free-standing GNR obtained from epitaxial graphene on a trenched substrate is a very interesting design that deserves a detailed investigation. However, it is known that phonons limit the carrier mobility and are thus relevant for transistor functions.^{12–14}

In this work, we use a continuum model to study the acoustic phonon properties of two different types of GNRs that we think can be realized in experiment: (i) extended graphene that covers a thin trench, resulting in a GNR parallel to the trench and with fixed lateral boundaries, Fig. [figure][1][1] (a); (ii) a strip of graphene that stretches over a wide trench, leading to a GNR perpendicular to the trench and with free lateral boundaries, Fig. [figure][1][1] (b). For both setups, we derive the low-energy acoustic phonon spectra from a continuum model that respects the monatomic structure of graphene and write down the quantum mechanical form of these phonons.

Our results can be probed experimentally via established techniques like electron energy loss spectroscopy or Brillouin light scattering.^{15,16} In addition to the electron mobility,¹⁷ the phononic behaviour is essential for carbon-based nanoelectromechanical systems.^{5,18} A recent example where the electron-phonon coupling has been observed experimentally is the Franck-Condon blockade in suspended carbon nanotube quantum dots.¹⁹ Phonons also give rise to spin relaxation within a time T_1 , which is important for spintronics devices, even in carbon-based systems where the intrinsic spin-orbit coupling is relatively weak.^{4,20–23} The effective spin-phonon interaction $H_{\text{s-p}}$ couples the Zeeman-split spin states (\uparrow, \downarrow) to the phonon bath with phonon numbers n_ω , into which the Zeeman energy $\hbar\omega$ is released. The rate for spin relaxation via emission of a phonon with

energy $\hbar\omega$ is given by

$$\frac{1}{T_1} = \frac{2\pi}{\hbar} |\langle \downarrow, n_\omega + 1 | H_{s-p} | \uparrow, n_\omega \rangle|^2 \text{DOS}(\hbar\omega), \quad (1)$$

with an explicit dependence on the phonon density of states, DOS.

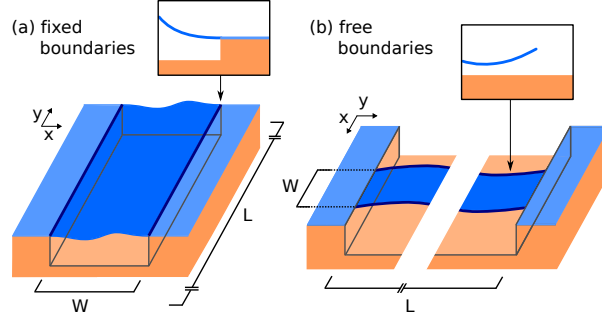


Figure 1: (Color online) We study two nanoribbon configurations where graphene (blue) is spanned over a trenched substrate (orange): (a) fixed and (b) free boundaries. The coordinate system is chosen in such a way that the undeformed ribbon lies in the xy -plane and that the y - and ribbon axes coincide. We assume the ribbon length to be much larger than the ribbon width ($L \gg W$) and parallel lateral boundaries (dark blue) at $x = \pm W/2$.

Low energy acoustic phonons at the center of the Brillouin zone have a wavelength much larger than atomic distances and thus can be derived from continuum mechanics. The carbon atoms in graphene lie within a two-dimensional surface and this property is conserved upon deformations, making graphene a quasi two-dimensional material in three-dimensional real space. Consequently, all components of the displacement field $\mathbf{u}(\mathbf{r}) = (u_x, u_y, u_z)$ can be nonzero but the components u_{iz} of the strain tensor $u_{ik} = (\partial_i u_k + \partial_k u_i)/2$ vanish identically. While u_{xz} and u_{yz} are known to vanish for thin plates in the xy -plane in general, the monatomic thickness of graphene implies that u_{zz} must vanish as well. The disappearance of u_{zz} becomes obvious when considering the relative volume change upon deformation, given by the trace u_{ii} : for a 2D lattice, there is no lowest order contribution from neighboring atoms shifting out-of-plane. With $u_{iz} \equiv 0$, the elastic Lagrangian density of monolayer graphene is given by^{24–27}

$$\mathcal{L} = \mathcal{T} - \mathcal{V} = \frac{\rho}{2} \dot{\mathbf{u}}^2 - \frac{\kappa}{2} (\Delta u_z)^2 - \frac{\lambda}{2} u_{ii}^2 - \mu u_{ik}^2, \quad (2)$$

where $\Delta = \partial_x^2 + \partial_y^2$, the sum convention with $u_{ii} = u_{xx} + u_{yy} + u_{zz}$ and $u_{ik}^2 = u_{xx}^2 + u_{xy}^2 + \dots$ has been used, ρ is the surface mass density and κ is the bending rigidity. Note that the 3D bulk elastic constants have been multiplied with the plate thickness h in order to yield the surface densities $\lambda = h\lambda_{3D}$ and $\mu = h\mu_{3D}$. The bulk and shear moduli are then given as $B = \lambda + \mu$ and μ , respectively.

Applying the Euler-Lagrange formalism to the functional (2) leads to the coupled set of differential equations for in-plane modes,

$$\begin{aligned}\rho \ddot{u}_x &= (B + \mu) \partial_x^2 u_x + \mu \partial_y^2 u_x + B \partial_x \partial_y u_y, \\ \rho \ddot{u}_y &= (B + \mu) \partial_y^2 u_y + \mu \partial_x^2 u_y + B \partial_x \partial_y u_x,\end{aligned}\tag{3}$$

which are decoupled from the differential equation for the out-of-plane modes,

$$\rho \ddot{u}_z = -\kappa (\partial_x^2 + \partial_y^2)^2 u_z.\tag{4}$$

Assuming nanoribbon alignment with the y -axis, fixed boundaries are described by $u_x = u_y = 0$ (in-plane) and $u_z = \partial_x u_z = 0$ (out-of-plane) at $x = \pm W/2$, see Fig. [figure][1][1] (a). While these boundary conditions hold for both, 2D and 3D lattices, we emphasize that lattice dimensionality does affect free boundaries. For free edges in 2D it is required that $(1 - \sigma) \partial_x u_x + \sigma \partial_y u_y = \partial_x u_y + \partial_y u_x = 0$ (in-plane) and $(1 - \sigma) \partial_x^3 u_z + (2 - 3\sigma) \partial_x \partial_y^2 u_z = (1 - \sigma) \partial_x^2 u_z + \sigma \partial_y^2 u_z = 0$ (out-of-plane), where the quantity σ denotes Poisson's ratio, Fig. [figure][1][1] (b).

Typically, the length of a graphene nanoribbon exceeds its width many times,^{9,28–30} $L \gg W$, thus allowing for a plane wave ansatz along the y -direction with periodic boundaries. Due to their decoupling, in plane modes $u_{x/y}(x, y, t) = f_{x/y}(x) \exp[i(qy - \omega t)]$ and out-of-plane modes $u_z(x, y, t) = f_z(x) \exp[i(qy - \omega t)]$ can be treated separately.

Exploiting the plane wave ansatz and denoting the i -th derivative of f as $f^{(i)}$, Eq. (3) can be

written as $\mathcal{M}_{xy}(f_x, f_y) = -\rho\omega^2(f_x, f_y)$, where

$$\mathcal{M}_{xy} : \begin{pmatrix} f_x \\ f_y \end{pmatrix} \mapsto \begin{pmatrix} (B + \mu)f_x^{(2)} - \mu q^2 f_x + iBqf_y^{(1)} \\ -(B + \mu)q^2 f_y + \mu f_y^{(2)} + iBqf_x^{(1)} \end{pmatrix}. \quad (5)$$

The general solution of this eigenvalue problem is $(f_x, f_y) = \sum_{i=1}^4 c_i \mathbf{a}_i \exp[\lambda_i x]$, with $\mathbf{a}_1 = (1, iq/\lambda_1)$, $\mathbf{a}_2 = (1, iq/\lambda_2)$, $\mathbf{a}_3 = (1, i\lambda_3/q)$, $\mathbf{a}_4 = (1, i\lambda_4/q)$ and

$$\lambda_{1,2} = \pm \sqrt{q^2 - \rho\omega^2/(B + \mu)}, \quad (6)$$

$$\lambda_{3,4} = \pm \sqrt{q^2 - \rho\omega^2/\mu}. \quad (7)$$

Fixed boundaries are characterized by $f_x(\pm W/2) = f_y(\pm W/2) = 0$ and by virtue of the λ_i , the set of linear equations deriving from these boundary conditions depends on parameters q and ω . A numerical treatment of this linear system yields the dispersion relation (Fig. [figure][2][2] (a, e)) as well as the coefficients c_i for the explicit form of the in-plane mode with fixed boundaries (Fig. [figure][3][3] (a, b)). Other boundary conditions and the out-of-plane modes can be treated likewise. The eigenvalue problem obtained from (4) is $\mathcal{M}_z f_z = (\rho\omega^2/\kappa - q^4)f_z$, where the map \mathcal{M}_z and its eigenfunctions and eigenvalues are given by

$$\mathcal{M}_z : f_z \mapsto f_z^{(4)} - 2q^2 f_z^{(2)}, \quad (8)$$

$$f_z = \sum_{i=1}^4 d_i e^{\lambda_i x} \quad (9)$$

$$\lambda_i = \pm \sqrt{q^2 \pm \omega \sqrt{\rho/\kappa}}. \quad (10)$$

A detailed discussion of the different phonon dispersion relations will follow further below.

In order to quantize the vibrational spectrum of the graphene nanoribbon in terms of phonon creation and annihilation operators, the eigenfunctions of the original differential operators (Eqs. (3) and (4)) must be orthonormal. While orthogonality of eigenmodes with different wavenumbers q follows from the plane wave ansatz, eigenmodes with same q require orthogonal functions

$(f_{(\alpha,q),x}, f_{(\alpha,q),y})$ and $f_{(\alpha,q),z}$. The index (α,q) labels the phonon branch α and the wavenumber q of a specific eigenmode. Normalization is trivial due to linearity of maps (5) and (8).

The map (5) is hermitian and hence has orthogonal eigenfunctions if and only if

$$\int_{-\frac{W}{2}}^{+\frac{W}{2}} dx (f_x^*, f_y^*) \cdot \mathcal{M}_{xy} \begin{pmatrix} f_x \\ f_y \end{pmatrix} \in \mathbb{R} \quad (11)$$

for all vector functions (f_x, f_y) in the domain of \mathcal{M}_{xy} . One easily shows via partial integration that \mathcal{M}_{xy} is hermitian if and only if the boundary terms satisfy

$$(B + \mu) f_x^* f_x^{(1)} + \mu f_y^* f_y^{(1)} + iBq f_x^* f_y \Big|_{-\frac{W}{2}}^{+\frac{W}{2}} \in \mathbb{R} \quad (12)$$

and that both, fixed and free boundaries do indeed satisfy this condition.

The general in-plane displacement field is a superposition of all in-plane eigenmodes,

$$\mathbf{u}_{\parallel} = \sum_{\alpha,q} r_{(\alpha,q)} (f_{(\alpha,q),x} \mathbf{e}_x + f_{(\alpha,q),y} \mathbf{e}_y) e^{iqy}, \quad (13)$$

where the harmonic time dependence has been absorbed in the normal coordinate. Using the orthonormality relations mentioned above, one can resolve the normal coordinate and derive the Lagrangian and the canonical momentum. The identification

$$r_{(\alpha,q)} = \sqrt{\frac{\hbar}{2\rho LW \omega_{(\alpha,q)}}} (b_{(\alpha,q)} + b_{(\alpha,-q)}^{\dagger}), \quad (14)$$

where $b_{(\alpha,q)}^{\dagger}$ ($b_{(\alpha,q)}$) creates (annihilates) an (α,q) -phonon, complies with coordinate-momentum commutation relations and allows for a quantum mechanical formulation of (13). Quantization of the out-of-plane modes is achieved in the very same way. The hermiticity of \mathcal{M}_z follows from

$$f_z^* f_z^{(3)} - f_z^{*(1)} f_z^{(2)} - 2q^2 f_z^* f_z^{(1)} \Big|_{-\frac{W}{2}}^{+\frac{W}{2}} \in \mathbb{R} \quad (15)$$

and as above, fixed as well as free boundaries do satisfy this condition. The general out-of-plane displacement is given by $\mathbf{u}_\perp = \sum_{\alpha,q} r_{(\alpha,q)} f_{(\alpha,q),z} \mathbf{e}_z e^{iqy}$ and (14) applies again.

We point out that specific values for sound velocities etc. in graphene depend on the elastic constants. Some of these constants remain unclear and seem to exhibit a temperature dependence, which we do not consider here. In the following, we use $\rho = 3.81 \times 10^{-7} \text{ kg/m}^2$, $B = 12.63 \text{ eV/\AA}^2$, $\mu = 9.15 \text{ eV/\AA}^2$, $\sigma = 0.16$, $\kappa = 1.1 \text{ eV}$ and $\mathcal{E} = \mathcal{E}_{3D}h = 3.4 \text{ TPa}\AA$, where \mathcal{E}_{3D} is Young's modulus of 3D graphite and $h = 3.4 \text{ \AA}$ is the graphite interlayer spacing.^{31–34}

Due to their decoupling, in-plane and out-of-plane phonons can be treated separately. For each case we discuss two different types of boundary conditions that we believe can be realized in experiment: fixed and free boundaries.

The dispersion relation of in-plane modes with fixed boundaries is gapped and features infinitely many branches with different energies originating from the zone center, Fig. [figure][2][2] (a, e). The gap relates to the energy necessary for fixing the boundaries and is given by $2.1 \hbar \sqrt{\mathcal{E}/\rho} / W$. For $W = 30 \text{ nm}$, this gap will be 1.4 meV . For large wavenumbers, all branches converge to a common line, which we label "TA". A second line, labelled "LA", is supported by different branches throughout the dispersion relation. Due to coupling at the ribbon boundaries there are no purely transverse or longitudinal modes. However, we do find that the modes on the TA (LA) line have predominantly transverse (longitudinal) character, Fig. [figure][3][3] (a, b). The corresponding sound velocities are $v_{\text{LA}} = 31 \text{ km/s}$ and $v_{\text{TA}} = 20 \text{ km/s}$, independent of the ribbon width. These values are comparable with previous calculations for bulk graphene (19.5 km/s , 12.2 km/s)³⁵ and carbon nanotubes (19.9 km/s , 12.3 km/s).²⁵ For the ratio $v_{\text{LA}}/v_{\text{TA}} = 1.6$, we even find very good agreement. We also want to point out that our sound velocities are proportional to $\sqrt{\mathcal{E}/\rho}$, a value that is still under discussion for graphene. The approach to linear, bulk-like behaviour is expected for large wavenumber, where the finite ribbon width appears like bulk for short wavelength phonons.

For free boundaries, the dispersion relation of in-plane modes is ungapped and the two branches that start at zero energy converge slightly below the TA line, Fig. [figure][2][2] (b, f). The sound

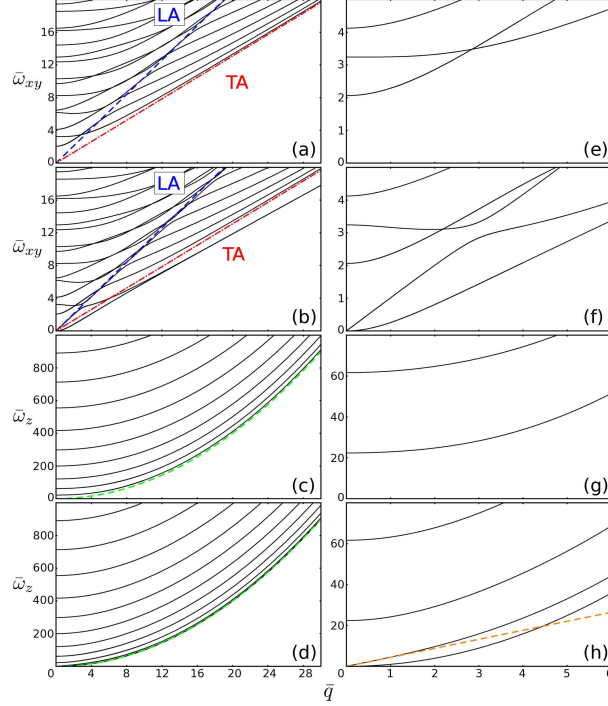


Figure 2: (Color online) Dispersion relations obtained from the procedure described in the text. The wavenumber q is given by $\bar{q} = qW$ and the frequency ω of in-plane (out-of-plane) phonons by $\bar{\omega}_{xy} = \omega\sqrt{\rho/\mathcal{E}W}$ ($\bar{\omega}_z = \omega\sqrt{\rho/\kappa W^2}$). (a) In-plane modes with fixed boundaries. (b) In-plane modes with free boundaries. (c) Out-of-plane modes with fixed boundaries. (d) Out-of-plane modes with free boundaries. (e-h) Dispersion relations (a-d) at the center of the Brillouin zone. (a, c, e, g) Modes with fixed boundaries exhibit a gap. (b, d, f, h) Modes with free boundaries are gapless. (a, b) Despite the coupling of transverse and longitudinal modes, we find predominantly longitudinal and transverse modes on lines which we label "LA" (dashed blue) and "TA" (dash-dotted red), respectively. (c, d) Independent of the boundaries, out-of-plane modes disperse quadratically for large wavenumbers (dashed green line). (h) Free out-of-plane modes feature a branch with linear dispersion at the zone center (dashed orange line).

velocities and linear behaviour for large wavenumber do not depend on boundary conditions, as one would expect with the same argument as above. Predominantly transverse and predominantly longitudinal modes are shown in Fig. [figure][3][3] (c, d). The typical zero point motion amplitude of in-plane modes is 50 fm.

The dispersion relation of out-of-plane modes with fixed boundaries is shown in Fig. [figure][2][2] (c, g). The gap due to the fixed boundary conditions is given by $22.4\hbar\sqrt{\kappa/\rho}/W^2$, which yields $11.1\mu\text{eV}$ for $W = 30\text{nm}$. There are infinitely many branches that correspond to different transverse excitations, Fig. [figure][4][4] (a, b). Again, away from the zone center, all

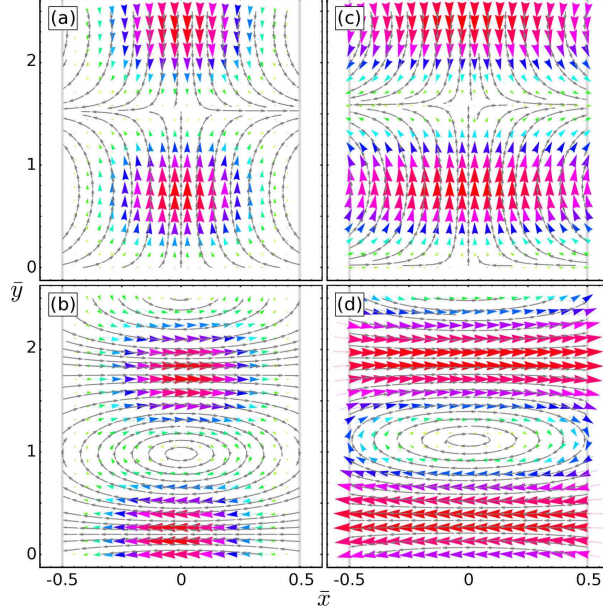


Figure 3: (Color online) In-plane modes can be illustrated as vector fields of the real part of (u_x, u_y) . Size and color of the arrows indicate the magnitude of the local deformation. We use the dimensionless coordinates $\bar{x} = x/W$ and $\bar{y} = y/W$. (a, b) Fixed boundaries. (c, d) Free boundaries. (a, c) Predominantly longitudinal modes. (b, d) Predominantly transverse modes.

branches approach bulk behaviour, that is a quadratic dispersion for out-of-plane modes.³⁵

Similarly, the out-of-plane modes with free boundaries disperse quadratically like bulk, for large wavenumbers, Fig. [figure][2][2] (d, h). The dispersion relation is gapless and one branch exhibits a finite sound velocity at the zone center. This sound velocity amounts to about 100 m/s for $W = 30$ nm, is proportional to $\sqrt{\kappa/\rho}/W$ and hence goes to zero for large W , again in agreement with bulk graphene. The typical zero point motion amplitude of out-of-plane modes is 0.6 pm.

Acoustic phonons are relevant for many GNR applications and can be probed with established techniques. Using a continuum model that accounts for the monatomic thickness of graphene, we derive boundary conditions that lead to hermitian wave equations. We focus on two types of boundary configurations, that we believe can be realized in experiment: fixed and free boundaries. We explicitly give the corresponding classical solutions and, exploiting hermiticity, infer a field theory with ribbon phonon creation and annihilation operators, thus allowing for a quantum mechanical treatment of acoustic graphene nanoribbon modes. Fixed boundaries lead to a gapped phonon dispersion relation of both in-plane and out-of-plane modes. In contrast, free boundaries

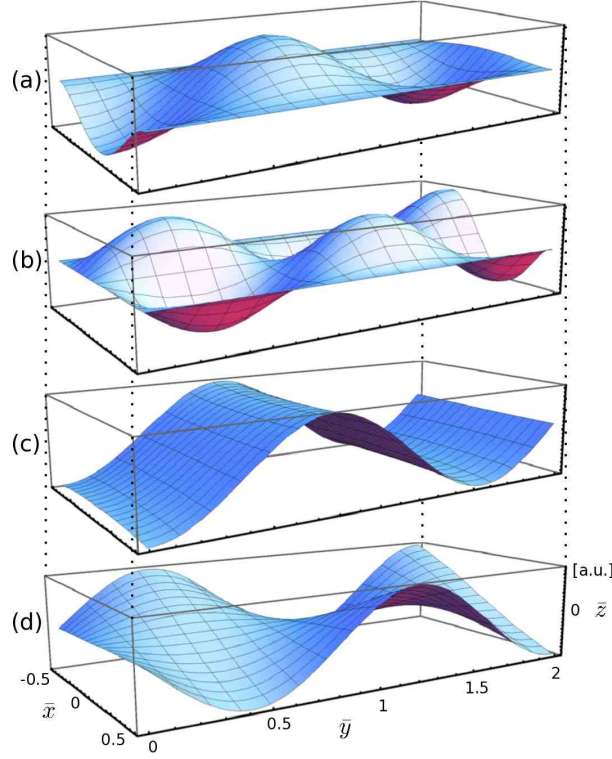


Figure 4: (Color online) Out-of-plane modes as real part of u_z . The dimensionless coordinates are $\bar{x} = x/W$, $\bar{y} = y/W$ and $\bar{z} = z/W$. (a, b) Fixed boundaries. (c, d) Free boundaries. (a, c) Fundamental mode. (b, d) First overtone.

lead to ungapped dispersion relations. Regardless of the boundary configuration, all dispersion relations approach bulk behaviour for wavelengths small compared to the ribbon width. Sound velocities that relate to transversal and longitudinal acoustical in-plane ribbon modes compare well with previous results for bulk graphene.

Acknowledgement

We thank András Pályi and Michael Pokojov for helpful discussions and acknowledge funding from the ESF within the EuroGRAPHENE project CONGRAN.

References

- (1) Novoselov, K. S.; Geim, A. K.; Morozov, S. V.; Jiang, D.; Zhang, Y.; Dubonons, S. V.; Grigorieva, I. V.; Firsov, A. A. *Science* **2004**, *306*, 666.

- (2) Lin, Y.-M.; Dimitrakopoulos, C.; Jenkins, K. A.; Farmer, D. B.; Chiu, H.-Y.; Grill, A.; Avouris, Ph. *Science* **2010**, 327, 662.
- (3) Lemme, M. C.; Echtermeyer, T. J.; Baus, M.; Kurz, H. *IEEE Electron Device Lett.* **2007**, 28, 282.
- (4) Trauzettel, B.; Bulaev, D. V.; Loss, D.; Burkard, G. *Nature Phys.* **2007**, 3, 192.
- (5) Garcia-Sanchez, D.; van der Zande, A. M.; San Paulo, A.; Lassagne, B.; McEuen, P. L.; Bachtold, A. *Nano Lett.* **2008**, 8, 1399.
- (6) Meyer, J. C.; Geim, A. K.; Katsnelson, M. I., Novoselov, K. S.; Booth, T. J., Roth, S. *Nature* **2007**, 446, 60.
- (7) Nair, R. R.; Blake, P; Grigorenko, A. N.; Novoselov, K. S.; Booth, T. J.; Stauber, T.; Peres, N. M. R.; Geim, A. K. *Science* **2008**, 320, 1308.
- (8) Bolotin, K. I.; Sikes, K. J.; Hone, J.; Stormer, H. L.; Kim, P. *Phys. Rev. Lett.* **2008**, 101, 96802.
- (9) Shivaraman, S.; Barton, R. A.; Yu, X.; Alden, J.; Herman, L.; Chandrasekhar, M.; Park, J.; McEuen, P. L.; Parpia, J. M.; Craighead, H. G.; Spencer, M. G. *Nano Lett.* **2009**, 9, 3100.
- (10) Lima, M. P.; Rocha, A. R.; da Silva, A. J. R.; Fazzio, A. *Phys. Rev. B* **2010**, 82, 153402.
- (11) Han, M. Y.; Özyilmaz, B.; Zhang, Y.; Kim, P. *Phys. Rev. Lett.* **2007**, 98, 206805.
- (12) Ouyang, Y.; Wang, X.; Dai, H.; Guo, J. *Appl. Phys. Lett.* **2008** 92, 243124.
- (13) Finkenstadt, D.; Pennington, G.; Mehl, M. J. *Phys. Rev. B* **2007** 76, 121405.
- (14) Farmer, D. B.; Chiu, H.-Y.; Lin, Y.-M.; Jenkins, K. A.; Xia, F.; Avouris, P. *Nano Lett.* **2009** 9, 4474.
- (15) Oshima, C.; Aizawa, T.; Souda, R.; Ishiziwa, Y. *Solid State Commun.* **1988**, 65, 1601.

- (16) Mohr, M.; Maultzsch, J.; Dobardžić, E.; Reich, S.; Milošević, I.; Damnjanović, M.; Bosak, A.; Krisch, M.; Thomsen, C. *Phys. Rev. B* **2007**, *76*, 035439.
- (17) Betti, A.; Fiori, G.; Iannaccone, G. *arXiv* **2011**, 1103.0295.
- (18) Steele, G. A.; Hüttel, A. K.; Witkamp, B.; Poot, M.; Meerwaldt, H. B.; Kouwenhoven, L. P.; van der Zant, H. S. J. *Science* **2009**, *325*, 1103.
- (19) Leturcq, R.; Stampfer, C.; Inderbitzin, K.; Durrer, L.; Hierold, C.; Mariani, E.; Schultz, M. G.; von Oppen, F.; Ensslin, K. *Nature Phys.* **2009**, *5*, 327.
- (20) Khaetskii, A. V.; Nazarov, Yu. V. *Phys. Rev. B* **2001** *64* 125316.
- (21) Kuemmeth, F.; Ilani, S.; Ralph, D. C.; McEuen, P. L. *Nature* **2008** *452*, 448.
- (22) Bulaev, D.; Trauzettel, B.; Loss, D. *Phys. Rev. B* **2008** *77*, 235301.
- (23) Struck, P. R.; Burkard, G. *Phys. Rev. B* **2010**, *82*, 125401.
- (24) Landau, L. D.; Lifshitz, E. M. *Theory of Elasticity*; Pergamon Press: New York, 1986.
- (25) Suzuura, H.; Ando, T. *Phys. Rev. B* **2002**, *65*, 235412.
- (26) Mariani, E.; von Oppen, F. *Phys. Rev. Lett.* **2008**, *100*, 76801.
- (27) Mariani, E.; von Oppen, F. *Phys. Rev. B* **2009**, *80*, 155411.
- (28) Li, X.; Wang, X.; Zhang, L.; Lee, S.; Dai, H. *Science* **2008**, *319*, 1229.
- (29) Jiao, L.; Zhang, L.; Wang, X.; Diankov, G.; Dai, H. *Nature* **2009**, *458*, 07919.
- (30) Kosynkin, D. V.; Higginbotham, A. L.; Sinitskii, A.; Lomeda, J. R.; Dimiev, A.; Price, B. K.; Tour, J. M. *Nature* **2009**, *458*, 07872.
- (31) Lee, C.; Wei, X.; Kysar, J. W.; Hone, J. *Science* **2008**, *321*, 385.
- (32) Kudin, K. N.; Scuseria, G. E.; Yakobsen, B. I. *Phys. Rev. B* **2001**, *64*, 235406.

- (33) Gazit, D. *Phys. Rev. B* **2009**, 79, 113411.
- (34) Fasolino, A.; Los, J. H.; Katsnelson, M. I. *Nature Mat.* **2007**, 6, 858.
- (35) Falkovsky, L. A. *Phys. Lett. A* **2008**, 372, 5189.